Efficient N_2 electroreduction enabled by linear charge transfer over atomically dispersed W sites

Jin Wan[a], Dong Liu[a], Chuanzhen Feng[a], Huijuan Zhang[a, b], Yu Wang[a, b*]*

[a] The School of Chemistry and Chemical Engineering, Chongqing University, 174 Shazheng Street, Shapingba District, Chongqing City, 400044, P.R. China

[b] College of Chemistry and Environmental Science, Inner Mongolia Normal University, Huhehaote, 010022, P. R. China

E-mail address: zhanghj@cqu.edu.cn ; *wangy@cqu.edu.cn*

Chemicals

V_2AlC MAX powder (≥ 98%, -200 mesh) was purchased from Beijing FUSIMAN Tech Co. Hydrofluoric acid (HF, 40.0% in aq. solution) was ordered from Chengdu Cologne Chemical Co. Tetrabutylammonium Hydroxide (TBAOH, 40% wt) was supplied from Shanghai Titan Scientific Co., Ltd. Tungsten chloride (WCl_6, 99.9% metals basis) was supplied from Shanghai McLean Biochemical Technology Co. All chemicals were used without any further purification.

Catalyst preparation

Synthesis of few-layer $V_{2-x}CT_y$ MXene

1.0 g of high-purity V_2AlC MAX powder was dispersed in 40 mL HF (40.0% in aq. solution). The etching process was stirred at room temperature for 36 h. The obtained $V_{2-x}CT_y$ powder was then exfoliated by sonication with TBAOH solution (3 days). Finally, the exfoliated $V_{2-x}CT_y$ powder was purified several times with distilled water and dried under vacuum for 12 h.

Synthesis of n-W/$V_{2-x}CT_y$

First, 100 mg $V_{2-x}CT_x$ MXene was dispersed in 40 mL distilled water and sonicated for 30 min to form solution A. Solution B was prepared by adding 10 mg of WCl_6 powder to 10 mL of ethanol and sonicated for 30 min**.** Then, solution B was slowly immersed in solution A and stirred for 12 h. Finally, the obtained n-W/$V_{2-x}CT_y$ was filtered and washed with distilled water for several times and dried under vacuum for one night.

Synthesis of WSAC/$V_{2-x}CT_y$

The synthesis of WSAC/$V_{2-x}CT_y$ follows a similar pathway as n-W/$V_{2-x}CT_y$, with the main difference being the reduced concentration of HF (30.0% in aq. solution) used to etch V_2CAl. The decrease in HF concentration reduces formation of V vacancy clusters, thereby diminishing the generation of W dual atoms.

Synthesis of W NPs/$V_{2-x}CT_y$

W NPs/$V_{2-x}CT_y$ was synthesized similarly to n-W/$V_{2-x}CT_y$, except for the added amount of WCl_6 powder (20 mg).

Characterization

X-ray diffraction (XRD) data were measured with Cu Kα radiation. X-ray photoelectron spectrometer (XPS, Thermo Scientific ESCALAB 250Xi spectrometer with an Al Kα radiation source) was adopted to determine the W atomic valence state. The metal loadings were tested by

ICP-MS on a VISTA MPX (Varian, Inc.). Field emission scanning electron microscopy (FESEM) and high-angle annular-dark-field scanning transmission electron microscopy (HAADF-STEM) images were performed on JEOL JSM-7800F at 15kV and Talos F200S at 200kV, respectively. The distribution states of W were characterized by an objective spherical aberration-corrected transmission electron microscopy (AC-TEM, FEI Titan ChemiSTEM). The X-ray absorption spectra of the W L3-edge were processed and fitted with Athena and Artemis programs and wavelet-transformed EXAFS plots were processed by Hama Fortran program.

Electrochemical measurements

The NRR measurements were tested on CHI 760E (CH Istruments, Inc., Shanghai) in an H-type cell with a three-electrode system. The as-prepared samples, Ag/ AgCl and Pt foil (1 cm × 1 cm) were the working electrode, reference electrode, and counter electrode, respectively. Before the test, the Nafion membrane was pretreated by boiling in H_2O_2 (3%) aqueous solution, 0.5 M H_2SO_4, and distilled water at 100 ℃ for 1.5 h. To prepare the working electrode, 5 mg of prepared samples were dispersed into 1000 μL ethanol containing 50 μL of 5 w% Nafion and sonicated for 1 h to obtain the catalyst ink. Subsequently, 80 μL of the n-W/ $V_{2-x}CT_y$ ink was loaded on the carbon paper (1 cm × 1 cm) and dried at room temperature. The electrode potentials were calibrated to the reversible hydrogen electrode (RHE) by using the following equation:

$$E_{RHE} = E_{Ag/AgCl} + 0.197 + 0.059 \times pH$$

Before electrochemical NRR measurement, all the electrolyte (0.05 M H_2SO_4 solution (pH=1)) was purged with high-purify N_2 (99.999%) for 30 min (flow rate: 20 mL min^{-1}).

Ammonia quantification

The concentration of produced NH_3 after electroreduction tests was detected by the indophenol blue method and NMR. For indophenol blue method, 2 mL solution was taken from the cathodic chamber and followed by adding 2 mL NaOH solution containing 5 wt% $C_7H_6O_3$, and 5 wt% $C_6H_5Na_3O_7$. Sequentially, 0.05 M NaClO (1 mL) and 1 wt% $C_5FeN_6Na_2O$ (0.2 mL) aqueous solution were added into the above mixed solution. After 2 h of reaction, the solution was measured at 655 nm using UV-Vis absorption spectra. For NMR, $^{15}N_2$ was used as the feeding gas, after 8 h of N_2 electroreduction, the electrolyte was taken out and further quantified by ^1H NMR.

Hydrazine quantification

The concentration of N_2H_4 electrolyte was determined by the method of Watt and Chrisp. Briefly, 5.99 g $C_9H_{11}NO$ and 30 ml of HCl in 300 ml ethanol were mixed and prepared as a color reagent. Then, 5 mL electrolyte was taken from the cathodic chamber and 5 mL color reagent was added. After the reaction for 20 min, the UV-Vis absorption spectra was measured at 458 nm.

Calculation of NH_3 yields and the Faradaic efficiency

The NH_3 yields were calculated by the following equation:

$$v_{NH_3} = (c_{NH_3} \times V)/(t \times m_{cat.})$$

The Faradaic efficiency (FE) was calculated as follows:

$$FE = (3 \times F \times c_{NH_3} \times V)/(17 \times Q)$$

where c_{NH_3} is the measured NH_4^+ concentration (μg mL^{-1}); V is the volume of electrolyte (mL); t is the electrolysis time (h); $m_{cat.}$ is the mass loading of the catalyst on the carbon paper; F is the faraday constant (96 500 C mol^{-1}); and Q is the quantity of applied electricity (C).

Computational Methods

All calculations were performed by spin polarization density functional theory (DFT) as implemented in the Vienna ab initio Simulation Package (VASP).[1-3] The core electrons were expanded by the Projected Augmented Wave (PAW) approach.[4] The generalized gradient approximation (GGA) with Perdew-Burke-Ernzerhof (PBE) functional was applied.[5] The DFT-D3 method was used to treat van der Waals (vdW) interactions in the systems.[6] A cutoff energy of 500 eV was applied for the plane-wave basis. The convergence criterion for energy and force were set to 10^{-5} eV and 0.03 eV/Å, respectively. A vacuum gap of 15 Å was utilized to avoid the interaction between the periodic images. The Brillouin zone was sampled using a 2×2×1 and 4×4×1 gamma (Γ) k-mesh for geometry optimization and electronic properties calculations, respectively. The Gibbs free energy change (ΔG) for each reaction was calculated by the formula:

$$\Delta G = \Delta E + \Delta E_{ZPE} + T\Delta S$$

Where ΔE, ΔE_{ZPE}, and ΔS are the changes of calculation energy, the zero-point energy difference, and the entropy change, respectively.

Furthermore, the limiting potential was calculated by the equation:

$$\eta^{NRR} = \Delta G/e.$$

The adsorption energy (E_{ads}) of adsorbate was calculated according to the equation:

$$E_{ads} = E_{sub/ads} - E_{sub} - E_{ads}$$

where $E_{sub/ads}$, E_{sub}, E_{ads} are energies of the substrate with adsorbate, the isolated substrate, and the corresponding adsorbate, respectively.

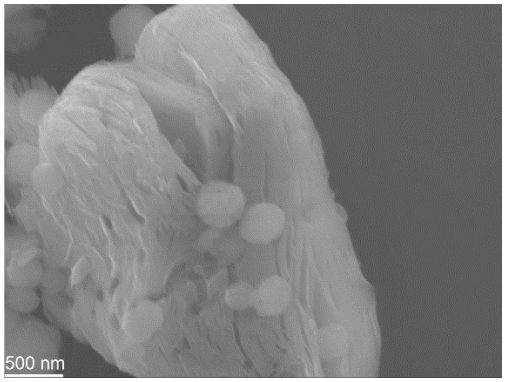

Figure S1. SEM image of multi-layer $V_{2-x}CT_y$ nanosheets.

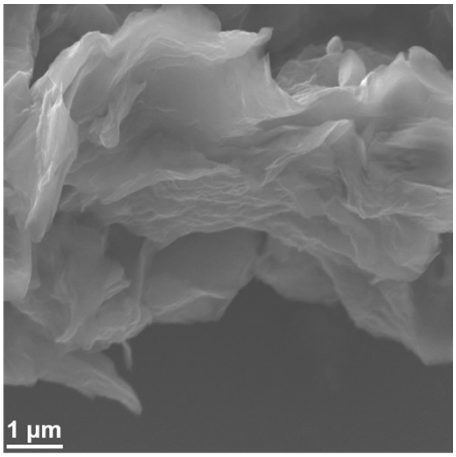

Figure S2. SEM image $V_{2-x}CT_y$ nanosheets after exfoliation.

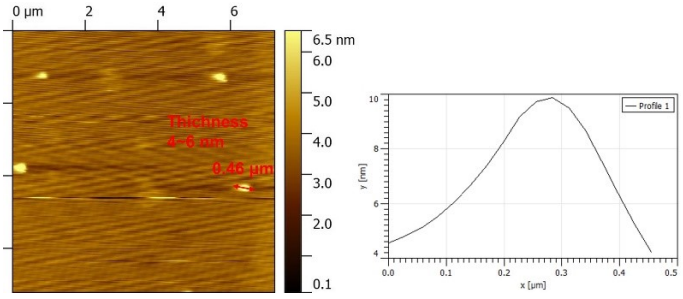

Figure S3. AFM image of $V_{2-x}CT_y$ nanosheets after exfoliation.

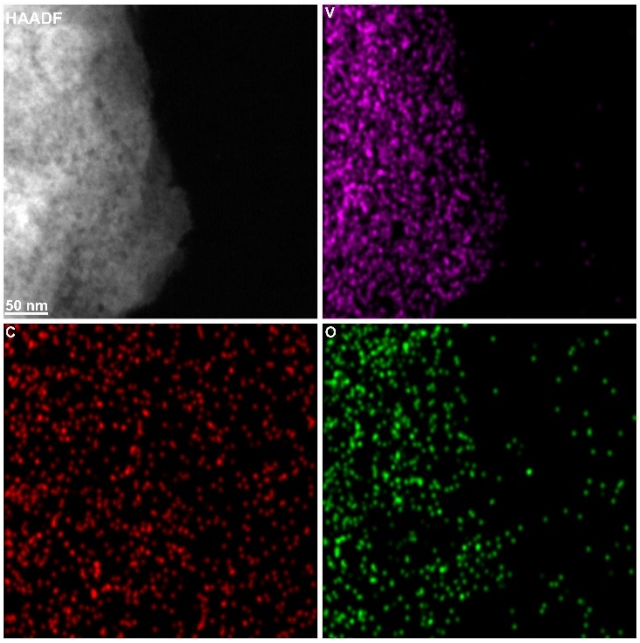

Figure S4. HAADF-STEM image and its EDS elemental mapping for elements V, C, and O of few-layer $V_{2-x}CT_y$ nanosheets.

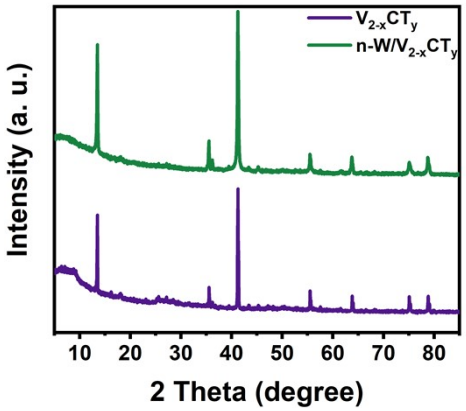

Figure S5. XRD diagrams of $V_{2-x}CT_y$ and n-W/$V_{2-x}CT_y$.

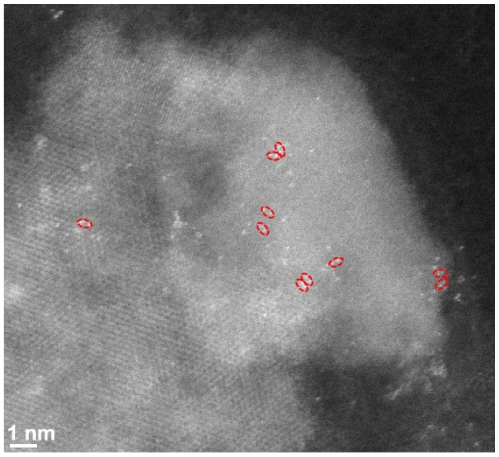

Figure S6. Atomic-resolution HAADF-STEM image of atomically dispersed W atoms on $V_{2-x}CT_y$ surface.

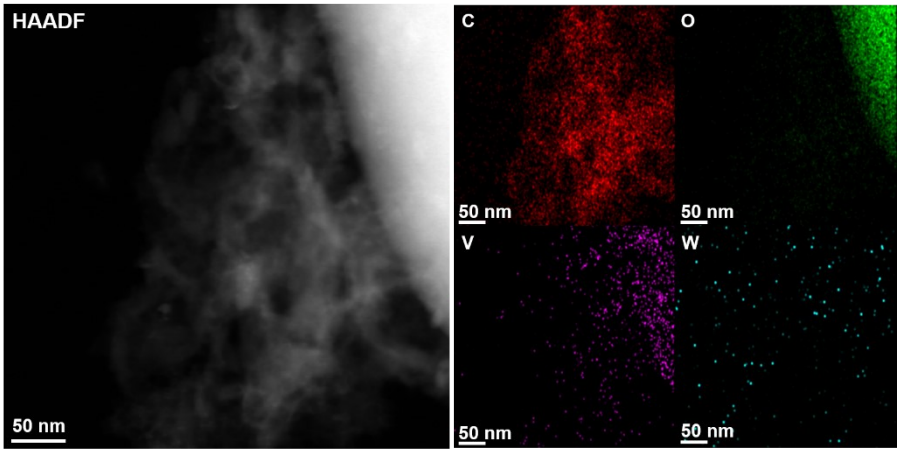

Figure S7. HAADF-STEM image and its EDS elemental mapping for elements V, C, O, and W of WSAC/$V_{2-x}CT_y$.

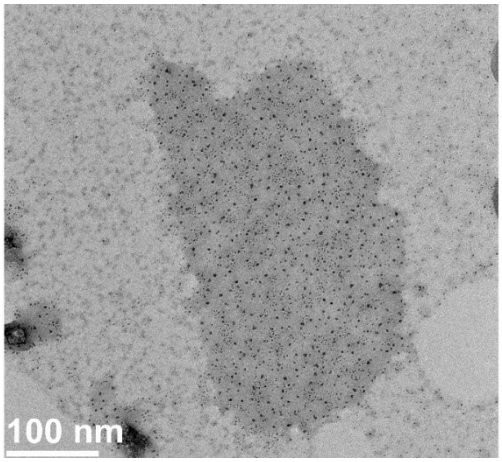

Figure S8. STEM image of W NPs/$V_{2-x}CT_y$.

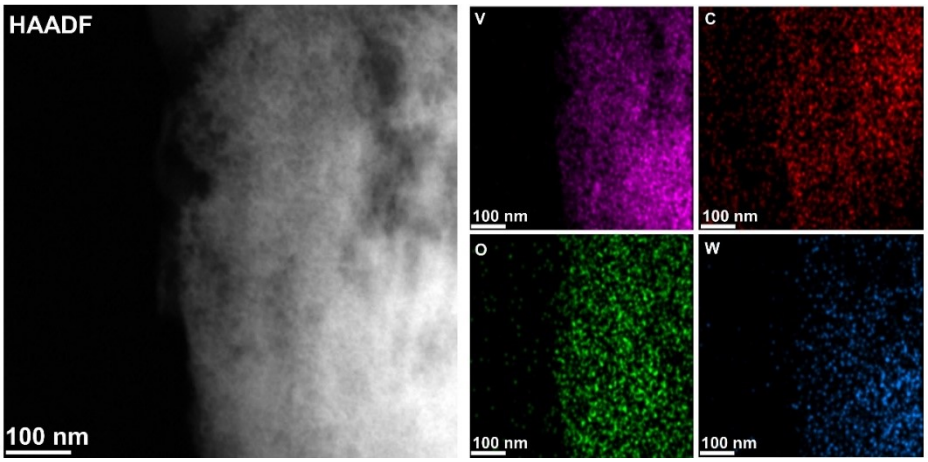

Figure S9. HAADF-STEM image and its EDS elemental mapping for elements V, C, O, and W of W NPs/$V_{2-x}CT_y$.

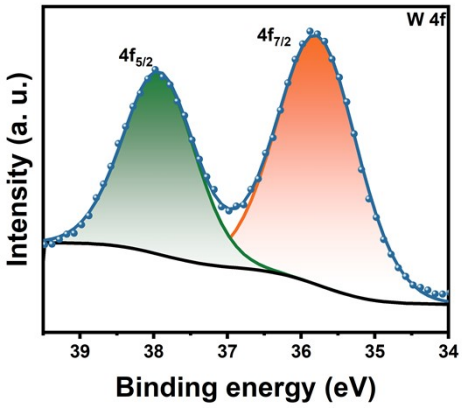

Figure S10. W 4f XPS spectrum of n-W/$V_{2-x}CT_y$.

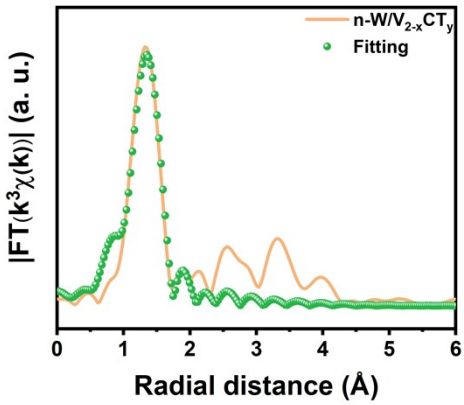

Figure S11. W K edge EXAFS fitting results in k space based on the theoretical model of WDAC/$V_{2-x}CT_y$ for n-W/$V_{2-x}CT_y$.

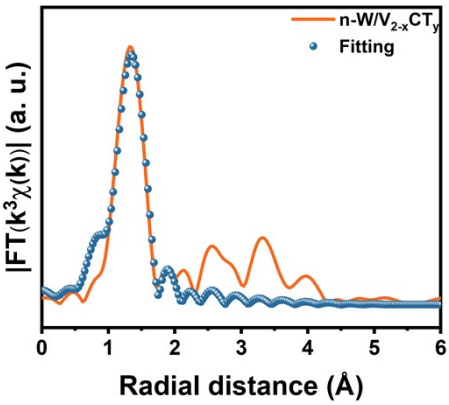

Figure S12. FT-EXAFS fitting results of n-W/$V_{2-x}CT_y$ in R space based on the theoretical model of WSAC/$V_{2-x}CT_y$.

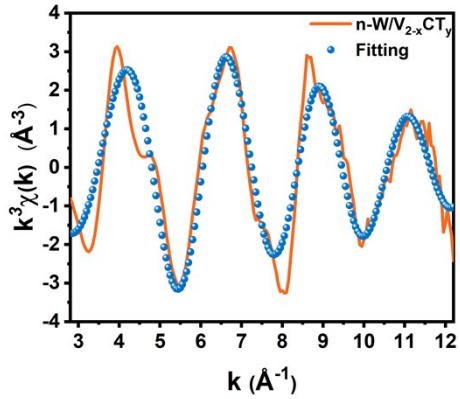

Figure S13. W K edge EXAFS fitting results in k space based on the theoretical model of WSAC/$V_{2-x}CT_y$ for n-W/$V_{2-x}CT_y$.

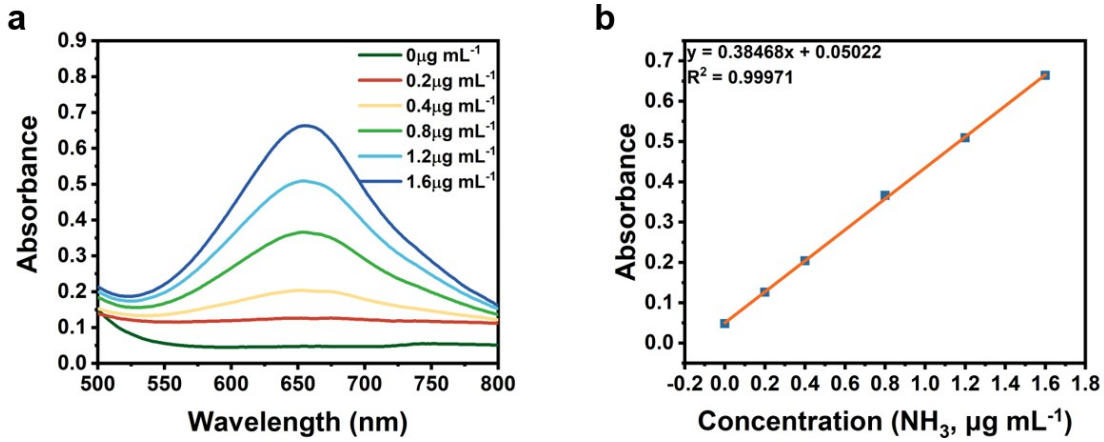

Figure S14. (a) UV-vis curves of indophenol assays with NH_4^+ ions (ammonium chloride solutions of known concentration) after being incubated for 2 h at room temperature. (b) calibration curve used for estimation of NH_3 by NH_4^+ ion concentration. The absorbance at 655 nm was measured by UV-vis spectrophotometer. The standard curve showed good linear relation of absorbance with NH_4^+ ion concentration ($y = 0.38468x + 0.05022$, $R^2 = 0.99971$).

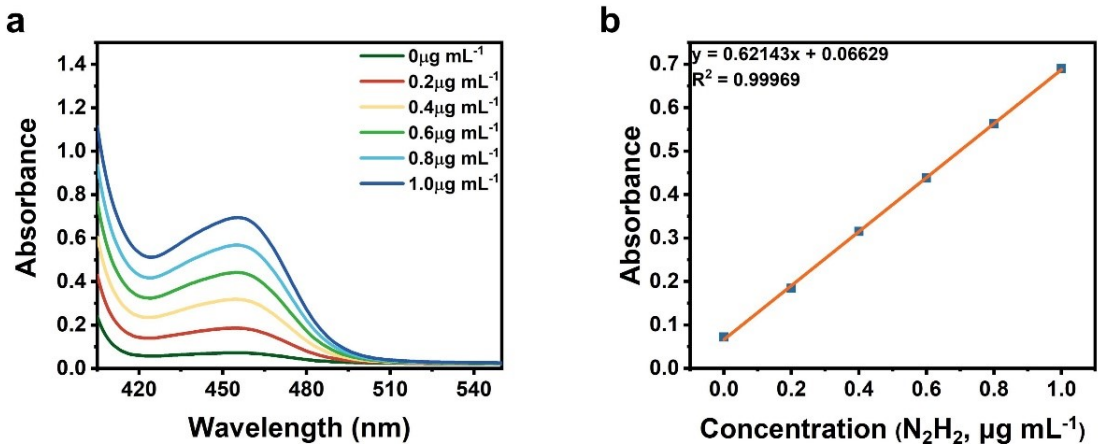

Figure S15. (a) UV-Vis absorption spectra of various N_2H_4 concentration after incubated for 20 min at room temperature. (b) Calibration curve used for calculation of N_2H_4 concentration. The absorbance at 458 nm was measured by UV-vis spectrophotometer. The standard curve showed good linear relation of absorbance with N_2H_4 ion concentration ($y = 0.62143x + 0.06629$, $R^2 = 0.99969$).

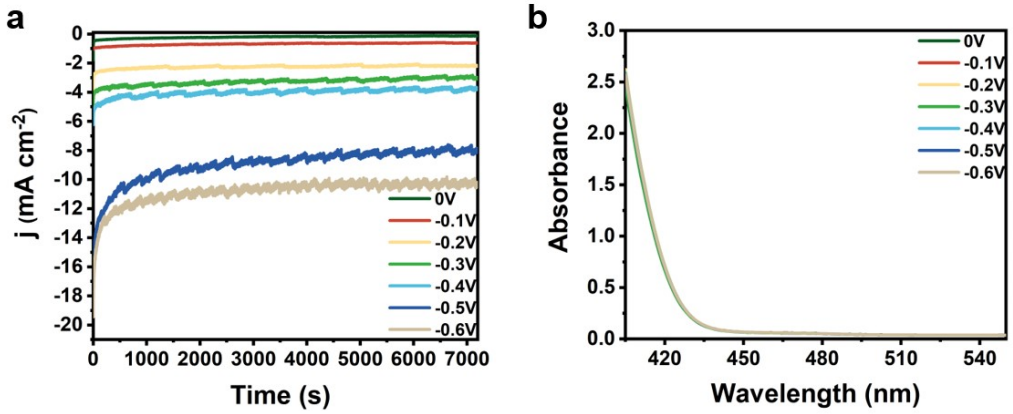

Figure S16. (a) Chronoamperometry curves of n-W/$V_{2-x}CT_y$ at different applied potentials in N_2-saturated 0.05 M H_2SO_4 solution. (b) UV-Vis absorption spectra of the electrolytes stained with para-dimethylamino-benzaldehyde indicator after 20 min electrolysis in N_2 at various potentials under ambient conditions.

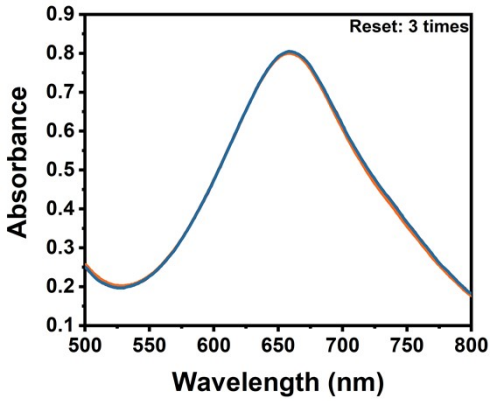

Figure S17. UV-Vis absorption spectra of n-W/$V_{2-x}CT_y$ at -0.1V (versus RHE) for 3 times.

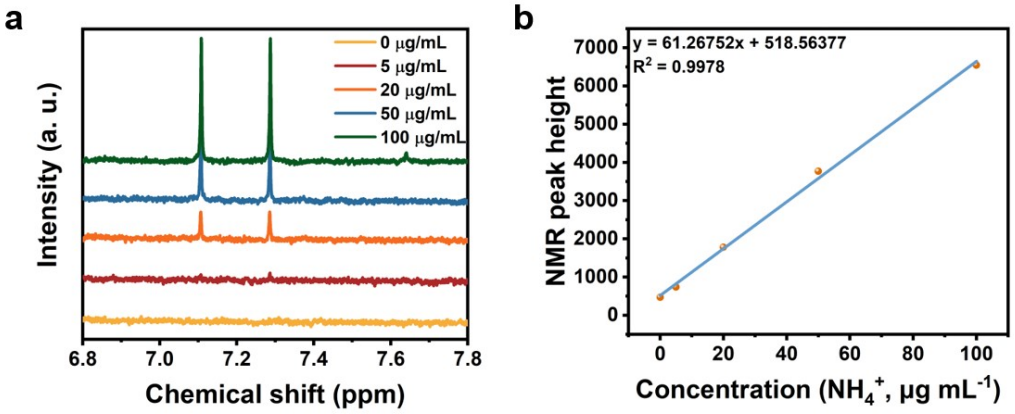

Figure S18. (a) ^{1}H NMR spectra of standard ammonia solution. (b) The standard curve of NMR peak height against NH_4^+ concentration.

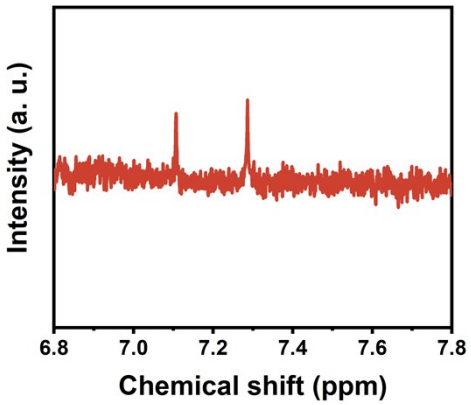

Figure S19. ^{1}H NMR spectra of the electrolyte over n-W/$V_{2-x}CT_y$ for NRR at -0.1 V (versus RHE) for 8 h.

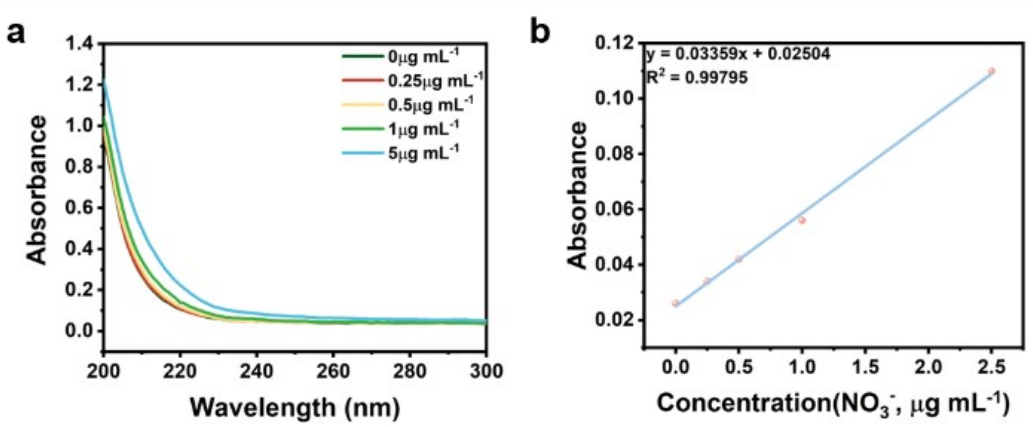

Figure S20. (a) UV-Vis absorption spectra of various NO_3^- concentration after incubated for 20 min at room temperature. (b) Calibration curve used for calculation of NO_3^- concentration.

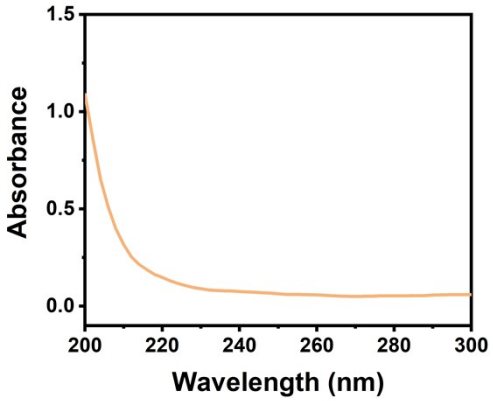

Figure S21. UV-Vis absorption spectra of NO_3^- for n-W/$V_{2-x}CT_y$ at -0.1 V (versus RHE).

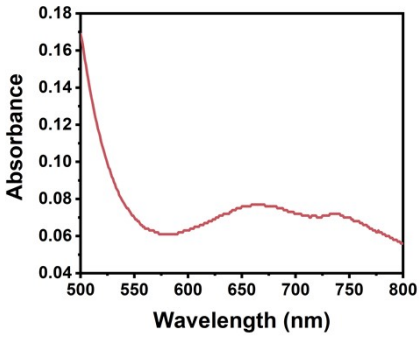

Figure S22. UV-Vis absorption spectra of NH_4^+ for n-W/$V_{2-x}CT_y$ at -0.1V (versus RHE) under Ar atmosphere.

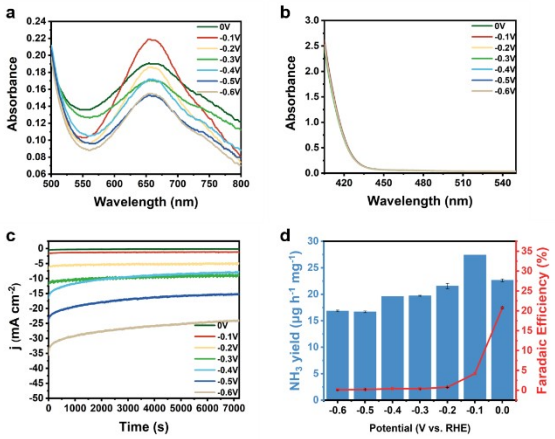

Figure S23. Electrochemical evaluation of $V_{2-x}CT_y$ (a) UV-Vis absorption spectra of indophenol assays with NH_4^+ after incubated for 2 h at different potentials. (b) UV-Vis absorption spectra of para-dimethylamino-benzaldehyde assays N_2H_4 after incubated for 20 min at different potentials. (c) Chronoamperometry curves of $V_{2-x}CT_y$ at different applied potentials in N_2-saturated 0.05 M H_2SO_4 solution. (d) NH_3 yields and FEs at different applied potentials.

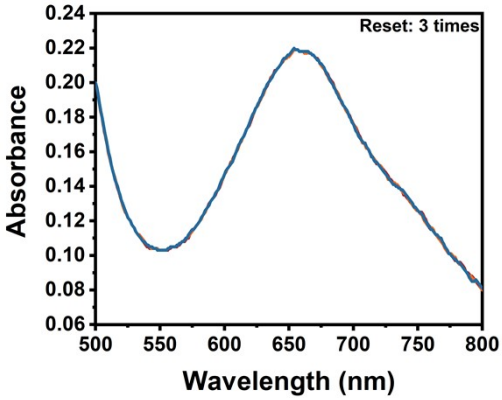

Figure S24. UV-Vis absorption spectra of $V_{2-x}CT_y$ at -0.1V (versus RHE) for 3 times.

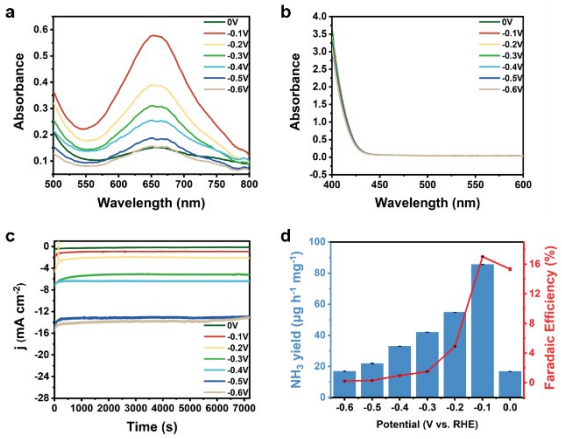

Figure S25. Electrochemical evaluation of WSAC/$V_{2-x}CT_y$ (a) UV-Vis absorption spectra of indophenol assays with NH_4^+ after incubated for 2 h at different potentials. (b) UV-Vis absorption spectra of para-dimethylamino-benzaldehyde assays N_2H_4 after incubated for 20 min at different potentials. (c) Chronoamperometry curves of WSAC/$V_{2-x}CT_y$ at different applied potentials in N_2-saturated 0.05 M H_2SO_4 solution. (d) NH_3 yields and FEs at different applied potentials.

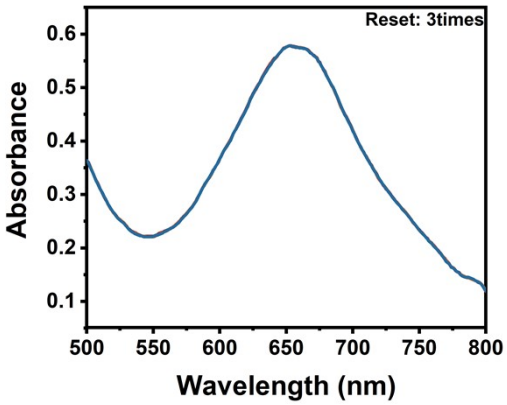

Figure S26. UV-Vis absorption spectra of $WSACV_{2-x}CT_y$ at -0.1V (versus RHE) for 3 times.

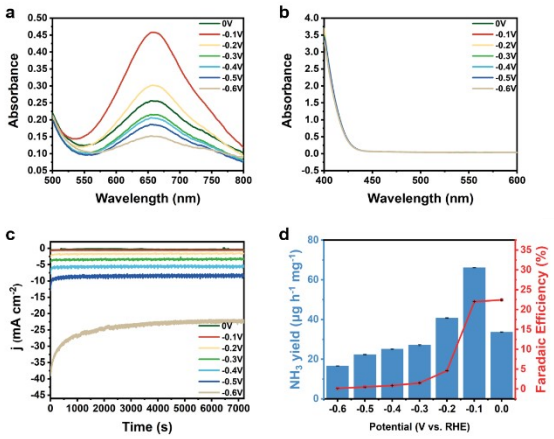

Figure S27. Electrochemical evaluation W NPs/$V_{2-x}CT_y$ (a) UV-Vis absorption spectra of indophenol assays with NH_4^+ after incubated for 2 h at different potentials. (b) UV-Vis absorption spectra of para-dimethylamino-benzaldehyde assays N_2H_4 after incubated for 20 min at different potentials. (c) Chronoamperometry curves of W NPs/$V_{2-x}CT_y$ at different applied potentials in N_2-saturated 0.05 M H_2SO_4 solution. (d) NH_3 yields and FEs at different applied potentials.

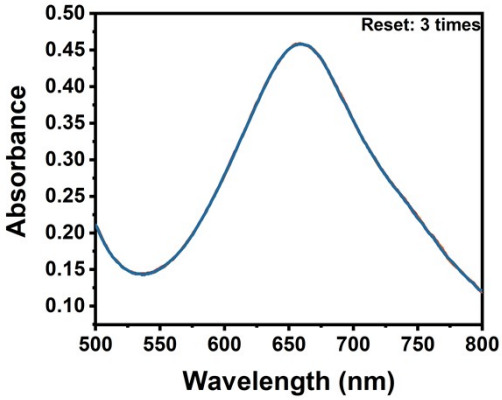

Figure S28. UV-Vis absorption spectra of W NPs/$V_{2-x}CT_y$ at -0.1V (versus RHE) for 3 times.

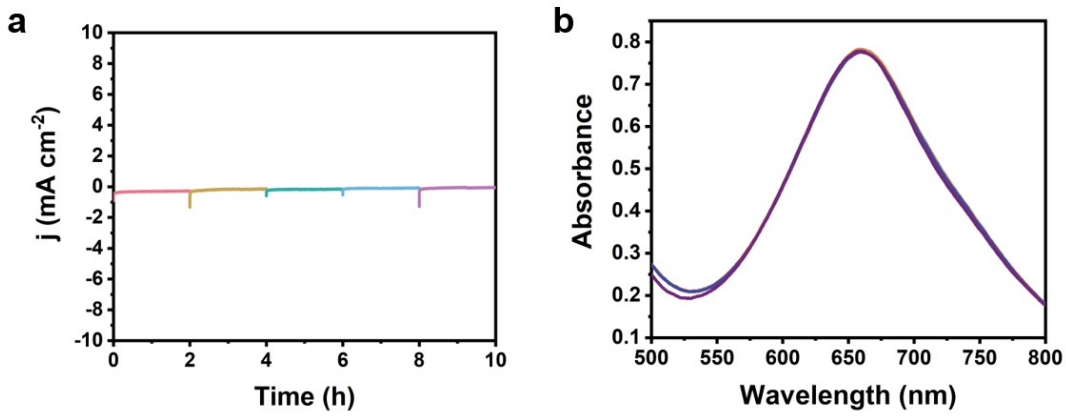

Figure S29. (a) Chronoamperometry curves in cycle tests of n-W/$V_{2-x}CT_y$ at -0.1V (versus RHE). (b) UV-Vis absorption spectra of indophenol assays in five cycles over n-W/$V_{2-x}CT_y$ at -0.1V (versus RHE).

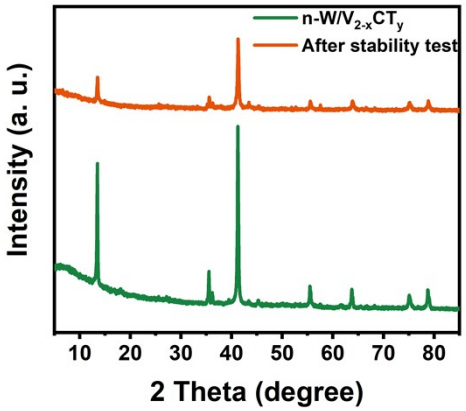

Figure S30. XRD diagrams of n-W/$V_{2-x}CT_y$ before and after stability test.

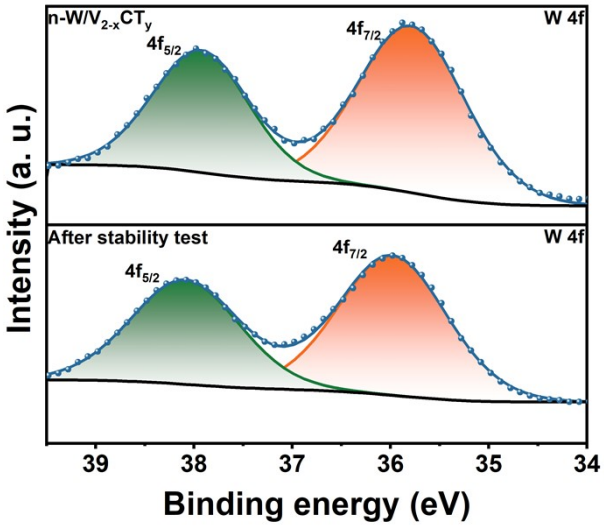

Figure S31. W 4f XPS spectrum of n-W/$V_{2-x}CT_y$ before and after stability test.

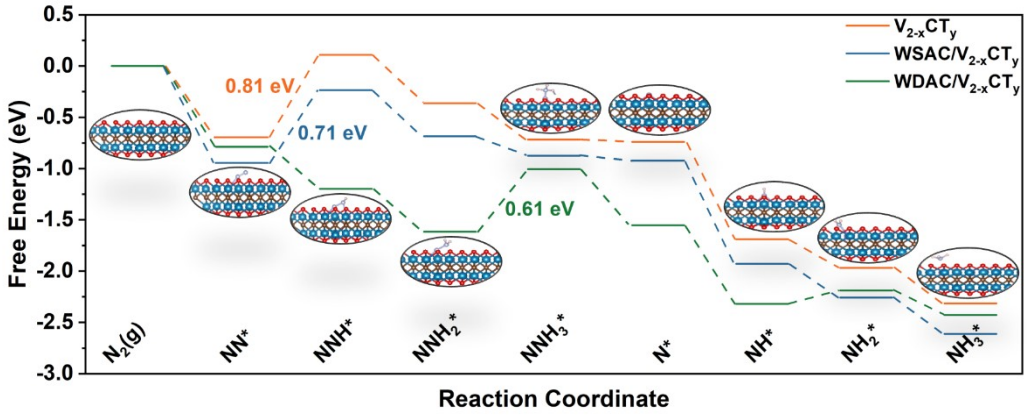

Figure S32. Gibbs free energy diagrams of NRR via distal pathways on $V_{2-x}CT_y$, $WSAC/V_{2-x}CT_y$, and $WDAC/V_{2-x}CT_y$, respectively.

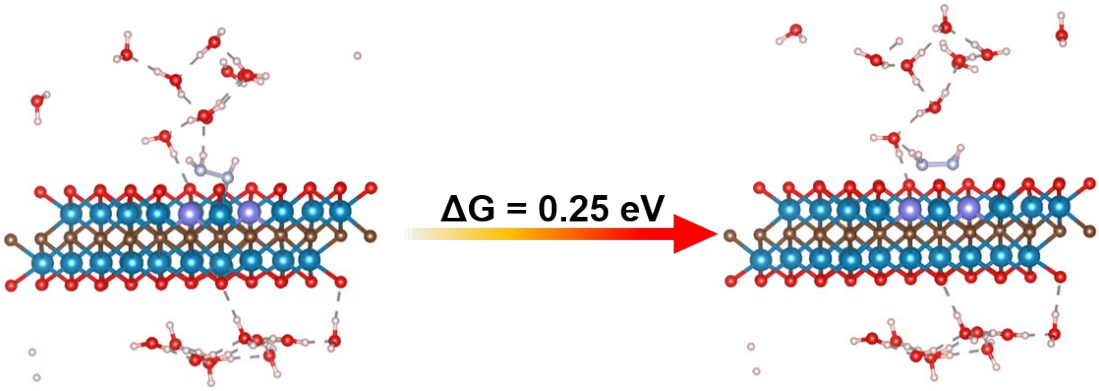

Figure 33. The explicit solvation model of $NHNH_2$ *→ NH_2NH_2 * step.

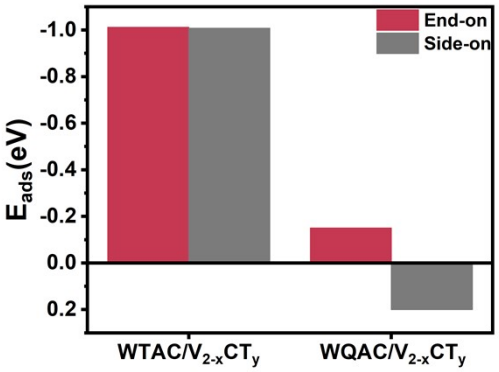

Figure S34. The adsorption energies of N_2 on WTAC/$V_{2-x}CT_y$, and WQAC/$V_{2-x}CT_y$ by side-on and end-on configurations, respectively.

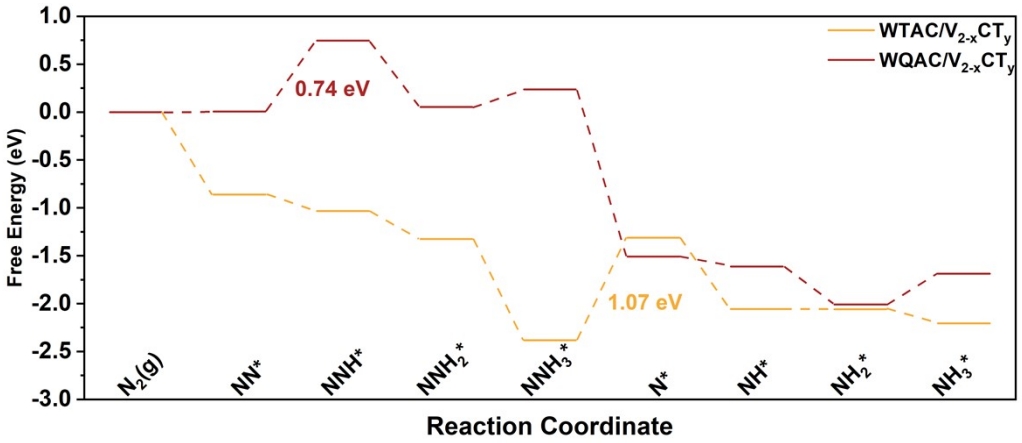

Figure S35. Gibbs free energy diagrams of NRR via distal pathways on WTAC/$V_{2-x}CT_y$, and WQAC/$V_{2-x}CT_y$, respectively.

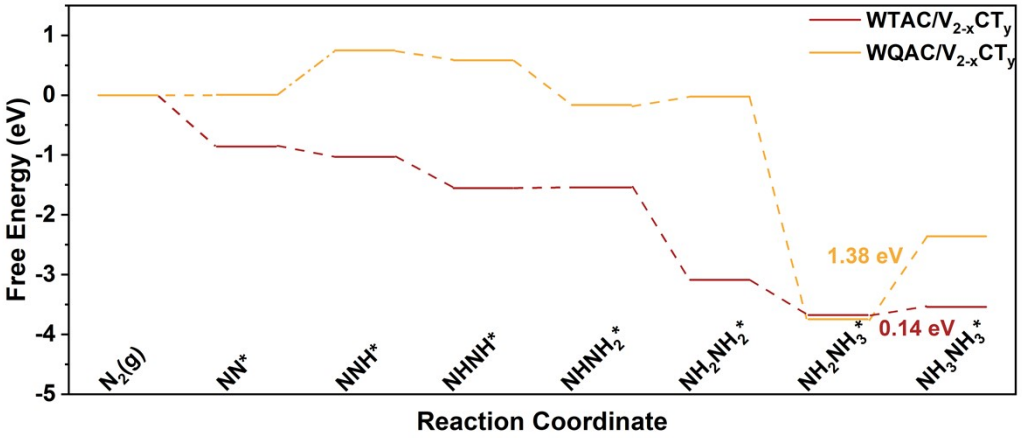

Figure S36. Gibbs free energy diagrams of NRR via alternating pathways on WTAC/$V_{2-x}CT_y$, and WQAC/$V_{2-x}CT_y$, respectively.

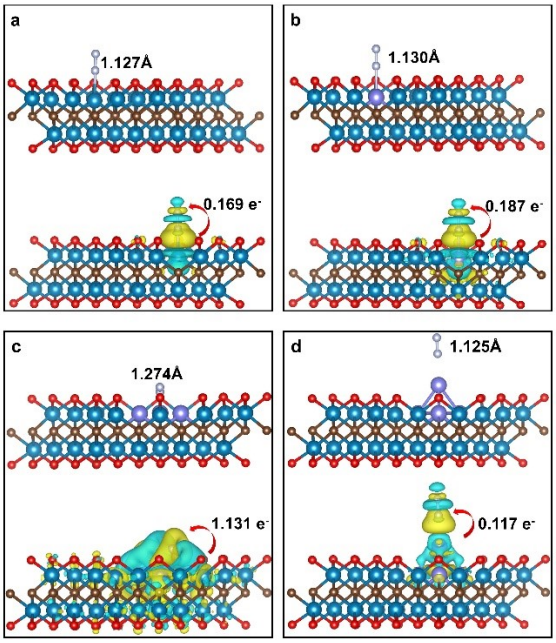

Figure S37. Optimized structures and charge density differences of N_2 on $V_{2-x}CT_y$, WSAC/$V_{2-x}CT_y$, WTAC/$V_{2-x}CT_y$, and WQAC/$V_{2-x}CT_y$ surfaces (Cyan and yellow represent charge depletion and accumulation, respectively. The isosurface value is 0.001 e/Å^3)

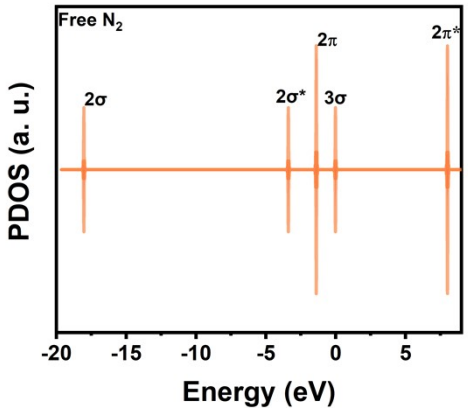

Figure S38. PDOS of free N_2.

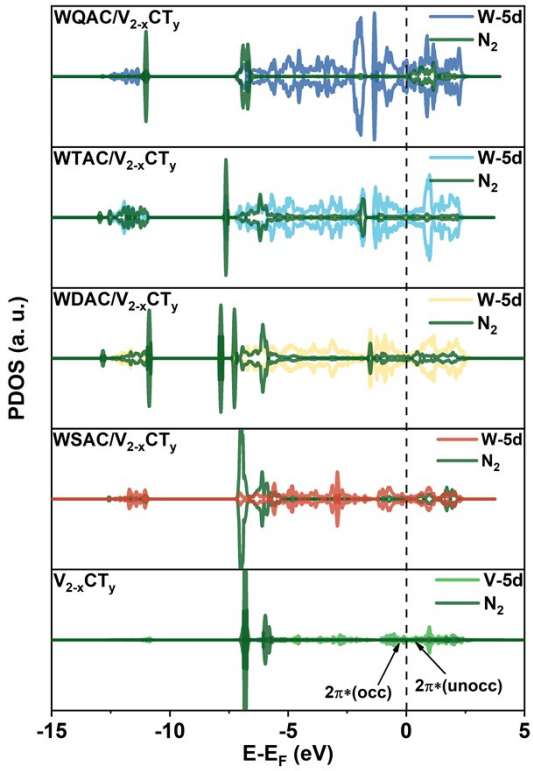

Figure S39. PDOS of N_2 on $V_{2-x}CT_y$, $WSAC/V_{2-x}CT_y$, $WDAC/V_{2-x}CT_y$, $WTAC/V_{2-x}CT_y$, and $WQAC/V_{2-x}CT_y$ surface.

TableS1. W loadings of the studied n-W/V_2CO_x catalyst and W NPs/ V_2CO_x, as determined by ICP-OES.

Catalysts	**Quality of WCl_6 (mg)**	**W loading (wt%)**
$V_{2-x}CT_y$	0	0
n-W/$V_{2-x}CT_y$	10 mg	1.39
W NPs/$V_{2-x}CT_y$	20 mg	5.12

TableS2. Curve fit parameters of W K-edge EXAFS based on WSAC/ $W/V_{2-x}CT_y$ and WDAC/ $W/V_{2-x}CT_y$ for n-$W/V_{2-x}CT_y$.

Sample	Path	N[b]	R(Å[c])	σ(10^{-3}Å^{2}[d])	ΔE_0(eV)	R factor
$WSAC/V_{2-x}CT_y$	W-C	3.62±0.72	1.97±0.02	5.06±3.1	-9.13±4.30	0.0189
$WDAC/V_{2-x}CT_y$	W-C	3.61±0.71	1.98±0.02	5.10±3.1	-9.22±4.25	0.0187

S_0^2 was fixed as 1.0. Data ranges $3.0 \leq k \leq 12.0$ Å^{-1}, $1.0 \leq R \leq 2.0$ Å. [b]N is the coordination number; [c]R is interatomic distance; [d]σ^2 is Debye-Waller factor; ΔE_0 is edge-energy shift. R factor is residual factor.

Table S3. Solvation energies (E_{solv}) of the catalytic reaction intermediates, η/vac and η/sol for the potential-limiting step of WDAC/$V_{2-x}CT_y$.

	E_{solv} (eV)	η/vac (eV)	η/sol (eV)
NN*	-0.52	-0.14	-0.41
NNH*	-0.66		
NHNHH*	-1.39	-0.77	0.32
NHHNHH*	-2.16		

References

1. G. Kresse and J. Furthmuller, *Comp. Mater. Sci.*, 1996, **6**, 15-50.
2. G. Kresse and J. Furthmuller, *Phys. Rev. B*, 1996, **54**, 11169-11186.
3. G. Kresse and D. Joubert, *Phys. Rev. B*, 1999, **59**, 1758-1775.
4. P. E. Blochl, *Phys. Rev. B*, 1994, **50**, 17953-17979.
5. J. P. Perdew, K. Burke and M. Ernzerhof, *Phys. Rev. Lett.*, 1996, **77**, 3865-3868.
6. S. Grimme, J. Antony, S. Ehrlich and H. Krieg, *J. Chem. Phys.*, 2010, **132**, 154104.